International Journal of the Physical Sciences Vol. 6(23), pp. 5528-5539, 9 October, 2011
Available online at http://www.academicjournals.org/IJPS
DOI: 10.5897/IJPS11.1431
ISSN 1992 - 1950 ©2011 Academic Journals

Full Length Research Paper

Automated surface micro flaw inspection for quality control of electronic chips

Hong-Dar Lin[1]* and Singa Wang Chiu[2]

[1]Department of Industrial Engineering and Management, Chaoyang University of Technology, 168 Jifong E. Road, Wufong District, Taichung 41349, Taiwan.
[2]Department of Business Administration, Chaoyang University of Technology, 168 Jifong E. Road, Wufong District, Taichung 41349, Taiwan.

Accepted 23 September, 2011

This research proposes a new approach that applies discrete cosine transform (DCT) based enhancement for the detection of micro flaws on electronic chips. A two-stage decomposition procedure is proposed to extract an odd-odd frequency matrix after a digital image has been transformed to DCT domain. The cumulative sum algorithm is then applied to detect the transition points of the gentle curves plotted from the odd-odd frequency matrix. After the transition points are determined, the proper radius of the cutting sector is computed and the high-pass filtering operation can be performed. The filtered image is then transformed back to the spatial domain. Thus, this study effectively attenuates the global random texture pattern and accentuates only micro flaws in the restored image. Finally, the restored image is segmented by an entropy method and some features of the detected flaws are extracted. Experimental results show that the proposed method achieves a high 96.24% probability of correctly discriminating micro flaws from normal regions and a low 0.15% probability of erroneously detecting normal regions as defects on random textured surfaces of electronic chips.

Key words: Industrial engineering, surface micro flaw inspection, electronic chips, quality control, machine vision.

INTRODUCTION

Surface defects affect not only the appearance of electronic devices but also their functionality, efficiency and stability. Large and obvious surface defects, such as indents, scraps and scratches are usually inspected by automated visual inspection systems. But surface micro flaws, such as dust, cavities and pinholes are very difficult to detect because of their extremely small sizes. Human visual inspections, commonly used today to detect surface micro flaws, are vulnerable to wrong judgments owing to inspectors' subjectivity and eye fatigues. Nevertheless, it is also hard to precisely inspect surface micro flaws by machine vision systems. When product images are being captured, the area of a micro flaw could expand, shrink or even disappear due to the uneven illumination of the environment, complex texture of the product surface, etc. To overcome the difficulties of inspecting micro flaws, this paper presents a computer vision-based quality system to automatically inspect micro flaws on surfaces of electronic chips.

Micro flaws, a common kind of surface defects, occur frequently in the manufacturing process and incur significant losses and damages. They exist on the surfaces of industrial parts, such as casting and steel as well as on those of high-tech products, such as wafer and electronic chip. Micro flaws cause much greater harms and impact, when they appear on high-tech products than on industrial parts. Although, micro flaws occupy only small areas on the product surface, they could affect the appearance, functions and security of the product. Even

*Corresponding author. E-mail: hdlin@cyut.edu.tw. Tel: 886-4-2332-3000. Ext. 4258. Fax: 886-4-2374-2327.

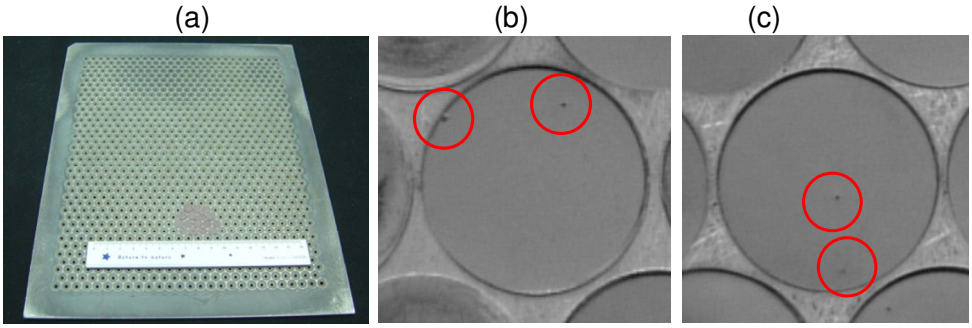

Figure 1. (a) An electronic chip carrier plate; (b) and (c) electronic chips with surface micro flaws.

a well-trained inspector cannot precisely identify the subtle micro flaws in a low-contrast surface.

This study uses round surface barrier layer chips as the testing samples. The electronic chips are ceramics capacitors which are one kind of electronic passive components commonly used in many electronic appliances. With a width of 0.005 mm and a diameter of 7 mm, the electronic chips are small in size, light in weight and suitable for mass and large-lot-sized production. Micro flaws often appear on the surfaces of electronic chips and occupy only extremely small areas. For an electronic chip image of 256 × 256 pixels, the size of its micro flaw falls within the range of 1 to 20 pixels and occupies 0.0015 to 0.0305% of the image area. Surface defects of this magnitude are defined as micro flaws in this research. Figure 1 shows (a) an electronic chip carrier plate used in the manufacturing process, (b) and (c) two images of electronic chips containing multiple micro flaws. Aiming to improve the inspection accuracy of surface micro flaws, this research proposes a discrete cosine transform (DCT) based enhancement approach to overcome the difficulties of traditional machine vision systems in detecting surface microflaws.

This research presents a global approach for the automated visual inspection of micro flaws on electronic chip surfaces. As common machine vision systems are not good at detecting micro flaws, we transform a digital image to DCT domain and analyze the energy trends of the frequency matrix. After some frequency components of the normal regions are removed, the rest of the components are transformed back to spatial domain to produce a restored image with enhanced micro flaws. These enhanced micro flaws can easily be separated from the normal regions by an entropy method.

In the aspect of defect detection, Kim et al. (1999) presented a new image contrast enhancing method based on the piecewise linear approximation of cumulative density function (CDF). Their method utilizes simplified histogram information obtained by the piecewise linear approximation to attain the controllability with much less effort. The major feature of this method is the controllability of the enhancement extent and partial adjustment. This method is an efficient and useful contrast tool with much reduced hardware for digital image display devices. Mak et al. (2009) proposed a feature based defect detection scheme applying morphological filters to tackle the problem of automated defect detection for woven fabrics. The important extracted features were used to facilitate the construction of structuring elements in subsequent morphological processing to remove the fabric background and isolate the defects.

Kim (1997) utilized mean preserving bi-histogram equalization method to do image enhancement. The mean of gray levels of an image is calculated as a threshold value to separate two regions for applying different histogram based enhancement methods. This method can avoid the loss of color information due to over-enhancement resulted from the large accumulation of a gray level. Ruzon and Tomasi (2001) used color distributions to detect edge, junction and corner. This research models a neighborhood as a distribution of colors. Their goal is to show that the increase in accuracy of this representation translates into higher-quality results for low-level vision tasks on difficult, natural images, especially as neighborhood size increases. Wu et al. (1996) developed an automated visual inspection system for printed circuit boards (PCBs). It utilized an elimination-subtraction which directly subtracts the template image from the inspected image, and then conducts an elimination procedure to locate defects in the PCB. This two-stage PCB automated inspection method is efficient, because only simple features are used to classify the defects.

With regard to techniques in the frequency domain, Chan and Pang (2000) used the Fourier transform to detect fabric defects. Tsai and Hsiao (2001) proposed a wavelet transform based approach for inspecting local defects embedded in homogeneous textured surfaces. By properly selecting the smooth sub-image or the combination of detail sub-images in different decomposition levels for backward wavelet transform, regular, repetitive texture patterns can be removed and only local anomalies are enhanced in the reconstructed image. Lin et al. (2011) proposed a new approach that applies block discrete cosine transform, Hotelling T2

statistic and grey clustering technique for the automatic inspection of visual defects in curved surfaces of LED lenses. Lin (2007) used the one-level Haar wavelet transform to decompose color images of surface barrier layer chips and extracted wavelet features from normal samples, and testing samples were statistically compared based on Hotelling, Mahalanobis and Chi-square distances to identify ripple blemishes on the chip images. The experimental results showed that Hotelling and Mahalanobis measures were superior in locating those ripple blemishes than Chi-square testing. Kumar (2008) and Ngan et al. (2011) surveyed and reviewed the articles related to fabric defect detection methods published in the last decades. These machine vision-based techniques were summarized, classified and commented in a comparison manner.

Use of the DCT in a wide variety of applications has not been as extensive as its properties would imply due to the lack of an efficient algorithm. Thus, many algorithms and very large-scale integration (VLSI) architectures for the fast computation of DCT have been proposed (Chen et al., 1977; Cho and Lee, 1991; Gonzalez and Woods, 2008). Chen et al. (1999) developed new and fast algorithms for edge enhancement of remote sensing image data in the DCT domain and implemented in three steps: high-pass filtering, adding back full or part of gray levels to the original image and contrast stretching. Experimental results show that the quality of images generated by the new algorithms is comparable with that of images generated by the corresponding methods in the spatial domain.

Zhong and Jain (2000) proposed an algorithm for object localization, using shape, color and texture. The texture and color features are directly extracted from the DCT compressed domain and are used to find a small number of candidate images in the database, and regions in the candidate images which share similar texture and color as the query can be identified. Experimental results demonstrate performance of the algorithm and show that substantial computational savings can be achieved by utilizing multiple image cues. Ngo et al. (2001) presented approaches for indexing shape, texture and color features directly in the DCT domain by exploiting ten DCT coefficients. For color and shape indexing, the proposed methods achieve significant speed up as compared to the same approach operating in the uncompressed image domain. Generally, the retrieval results are competent since most of the top retrieved images are relevant.

METHODOLOGY

Automated flaw detection approaches can be divided into two types. Methods of the first type choose and calculate a set of textural features in a sub-image and then, compare the feature values with those of the normal reference image to find significant differences. Disadvantages of the first type include: difficulties in deciding what valuable features to extract for texture discrimination, time consuming of the training process for the addition of a new textural feature and sophisticated classifiers needed to discriminate texture classes when a vector of multiple features results in high dimensionality (Tsai and Hsiao, 2001). Methods of the second type, detect flaws by comparing the testing image with a normal reference image by a template-to-template matching process. Disadvantages of the second type include: time consuming of the matching process, sensitivity to noises and large data storage needed for the pre-stored templates and the matching process (Lin, 2007).

This research applies DCT and cumulative sum algorithm to detect micro flaws in electronic chip surfaces. A product image is transferred from spatial domain to frequency domain by discrete cosine transform. Then, a two-stage decomposition procedure is proposed to analyze the energy trend of a frequency matrix. The first stage decomposes a two-dimensional discrete cosine spectrum into three one-dimensional frequency matrices. The second stage further decomposes the three frequency matrices to produce a principal frequency matrix for energy trend analysis. The cumulative sum (CUSUM) algorithm is applied to find the transition points of the gradual curves plotted by the principal datum of the decomposed frequency matrix and to determine the proper cutting sector radius. After frequency components within the proper radius of the cutting sector are removed, the frequency domain image is transferred back to the spatial domain and the micro flaws are apparently enhanced. Then, an image segmentation technique, entropy method, is applied to separate the defects from normal regions.

DCT and frequency domain analysis

Since digital images are two dimensional discrete data arrays, two dimensional DCT transform is needed to process the transformation. The DCT of an image $d_{x,y}$ of size $M \times N$ is given by Equation 1 (Ahmed et al., 1974). This expression must be computed for values of $u = 0, 1, 2, \ldots, M-1$, and also for $v = 0, 1, 2, \ldots, N-1$. Similarly, given $D_{u,v}$, we obtain $d_{x,y}$ via the inverse DCT transform, given by the Equation 2 for $x = 0, 1, 2, \ldots, M-1$ and $y = 0, 1, 2, \ldots, N-1$. Equations 1 and 2 comprise the two-dimensional, DCT pair. The variables u and v are frequency variables, and x and y are spatial variables.

$$D_{u,v} = \rho(u)\rho(v)\sum_{x=0}^{M-1}\sum_{y=0}^{N-1} d_{x,y}\cos\left[\frac{(2x+1)u\pi}{2M}\right]\cos\left[\frac{(2y+1)v\pi}{2N}\right] \quad (1)$$

$$d_{x,y} = \sum_{u=0}^{M-1}\sum_{v=0}^{N-1}\rho(u)\rho(v)D_{u,v}\cos\left[\frac{(2x+1)u\pi}{2M}\right]\cos\left[\frac{(2y+1)v\pi}{2N}\right] \quad (2)$$

where

$$\rho(u) = \begin{cases}\sqrt{\frac{1}{M}}, & u=0\\ \sqrt{\frac{2}{M}}, & u=1,2,3,\ldots,M-1\end{cases}, \quad \rho(v) = \begin{cases}\sqrt{\frac{1}{N}}, & v=0\\ \sqrt{\frac{2}{N}}, & v=1,2,3,\ldots,N-1\end{cases}, \quad \begin{cases}u=0,1,2,\ldots,M-1\\ v=0,1,2,\ldots,N-1\\ x=0,1,2,\ldots,M-1\\ y=0,1,2,\ldots,N-1\end{cases}.$$

Based on the fluctuations of energy trend and the properties of low and high frequency zones, a high-pass sector filter centered at the origin of the 2-D DCT spectrum was designed to filter out the major frequency components of the target. An adequate radius is first determined for the sector filter in the spectrum space. Frequency components (low frequencies) within the radius of the sector filter

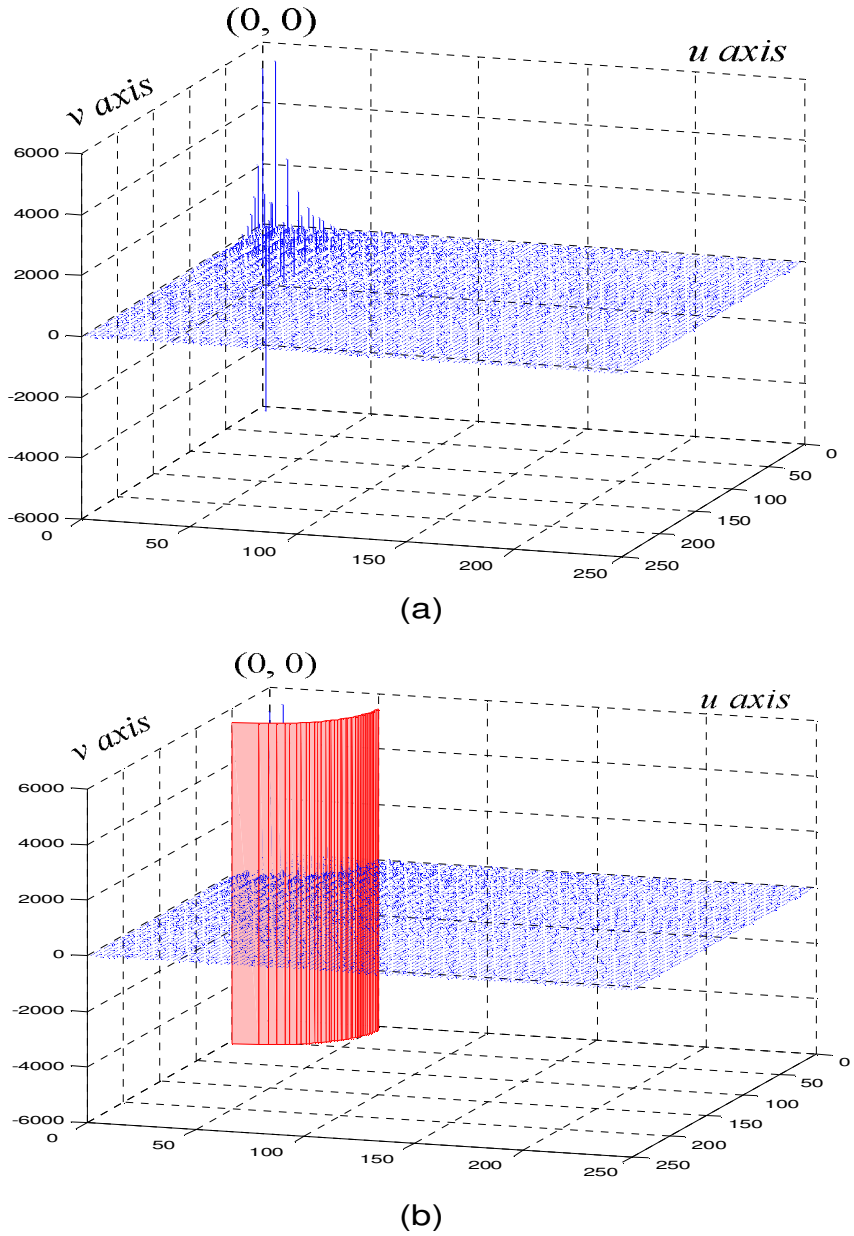

Figure 2. A high-pass sector filter added into a 3-D DCT spectrum diagram: (a) A 3-D diagram of a DCT spectrum; (b) A 3-D diagram of a DCT spectrum with a cutting sector radius.

are then set at zero, and those outside the filter (medium and high frequencies) are retained. Finally, the inverse DCT is used to enhance the surface micro flaws. Figure 2 demonstrates a 3-D DCT spectrum diagram with a high-pass sector filter.

As the high-pass sector filter is derived from the decreasing energy trend of the DCT spectrum diagram, conducting a proper analysis on the fluctuation trend of the energy spectrum carries great importance. It takes little effort to observe the energy trend from 2-D spectrum diagrams. But, a formal algorithm deduction must be carefully developed if the frequency spectrum diagram is to be analyzed from an objective and theoretic view. To construct the analysis steps of the DCT spectrum, this research analyzes the 2-D DCT spectrum and proposes a two-stage decomposition procedure. Due to the difficulty of analyzing the frequency fluctuation trend in a 3-D spectrum diagram, this research decomposes a 2-D DCT spectrum into 1-D frequency arrays to discover the regular patterns of the spectrum in the frequency domain.

Frequency trend analysis of DCT domain

Let *G** be a waveform sign of 1-D frequency arrays and axis be a 1-D coordinate vector. Then, *G*(axis)* is a waveform plot along the *axis* coordinate and can be denoted as:

$$G^*(axis) = D_{u,v}^{\#1} \tag{3}$$

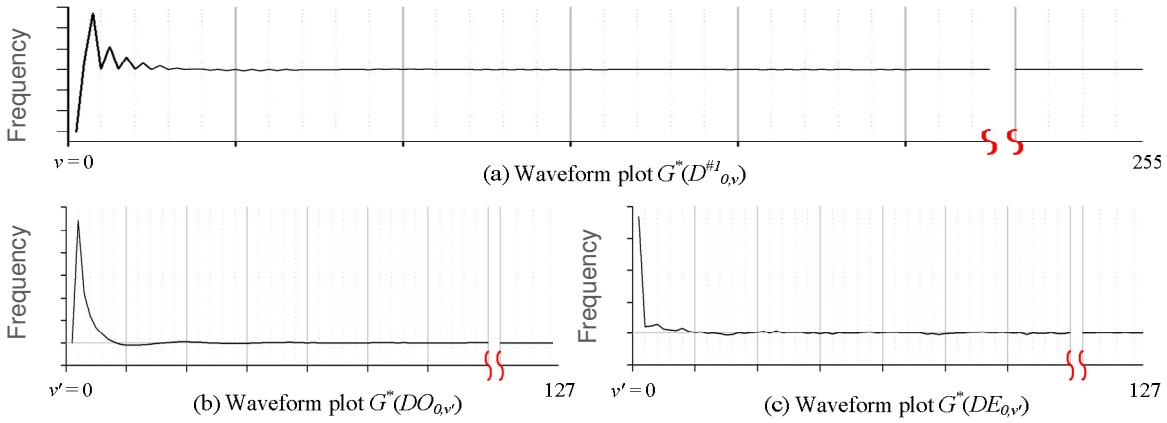

Figure 3. Three waveform plots of the $D^{\#1}_{0,v}$, $DO_{0,v'}$ and $DE_{0,v'}$.

where

$$\begin{cases} axis = D^{\#1}_{u,0\sim(N-1)} \text{ or } D^{\#1}_{0\sim(M-1),v} \\ u = 0, 1, 2, ..., M-1 \\ v = 0, 1, 2, ..., N-1. \end{cases}$$

The magnitude of frequency components far away from the top left origin in the DCT domain falls rapidly and approximates zero, because most image information gathers around the DC location and the waveforms fluctuate most widely there. The waveforms of $G^*(D^{\#1}_{0\sim(M-1),v})$ remain more and more stable as the values of the u axis increase. The same phenomenon also happens to the waveform plots of $G^*(D^{\#1}_{u,0\sim(N-1)})$.

The complexity of 2-D DCT domain makes it difficult to comprehend; whereas, by applying Equation 3, a 2-D DCT domain can be decomposed into the 1-D waveform matrices, in which systematic and regular patterns can be found. Hence, to take the advantage of decomposition and dig out more useful information, this research further decomposes the 2-D DCT domain to detect the changes of frequency trends.

Decomposition of DCT domain

The waveforms of $G^*(D^{\#1}_{0\sim(M-1),v})$ of 2-D DCT frequency components fluctuate as they approach the DC location, and the closer the waveforms are to the DC location, the more widely they fluctuate. We decide to further decompose the 2-D DCT domain $D^{\#1}_{u,v}$ into two matrices: the odd matrix $DO_{u,v'}$ and the even matrix $DE_{u,v'}$, whose definitions are given as follows:

$$DO_{u,v'} = D^{\#1}_{u,2v'}, \quad (4)$$

$$DE_{u,v'} = D^{\#1}_{u,2v'+1}, \quad (5)$$

where

$$\begin{cases} u = 0, 1, 2, ..., M-1 \\ v' = 0, 1, 2, ..., (N/2)-1 \end{cases}.$$

Based on the definitions of odd and even frequency matrices as shown in Equations 4 and 5, waveform plots $G^*(DO_{0\sim(M-1),v'})$ and $G^*(DE_{0\sim(M-1),v'})$ were used to examine their respective 1-D waveforms. We find some waveform regularities among the frequency fluctuations in the decomposed odd and even frequency matrices. Taking the waveform plots $G^*(DO_{0,v'})$ and $G^*(DE_{0,v'})$ as examples, the waveform plots of $D^{\#1}_{0,v}$, $DO_{0,v'}$ and $DE_{0,v'}$ were as shown in Figure 3.

As shown in Figure 3, after $D^{\#1}_{u,v}$ is decomposed into $DO_{u,v'}$ and $DE_{u,v'}$, the frequencies of the waveform plots $G^*(DO_{0,v'})$ and $G^*(DE_{0,v'})$ become more stable and steady; they do not fluctuate as much as before the decomposition. This phenomenon occurs not only in $G^*(DO_{0,v'})$ and $G^*(DE_{0,v'})$, but also in waveform plots $G^*(DO_{1\sim(M-1),v'})$ and $G^*(DE_{1\sim(M-1),v'})$. These occurrences lead to the conclusion that the coefficients of the DCT domain have a lot to do with whether the basic cosine waveform matrices have complete or incomplete periods. Examining the waveforms of $G^*(DO_{u,0\sim(N/2)-1})$ and $G^*(DE_{u,0\sim(N/2)-1})$, we find no similar phenomenon. The frequencies do not become more stable or steady, because the u axis of the DCT frequency matrix has not been decomposed. Therefore, the original frequency matrix $D^{\#1}_{u,v}$ can further be decomposed into odd-odd $DOO_{u',v'}$, odd-even $DOE_{u',v'}$, even-odd $DEO_{u',v'}$ and even-even $DEE_{u',v'}$ matrices under the alternating decomposition of odd and even parts. These four matrices can be denoted as follows, respectively:

$$DOO_{u',v'} = D^{\#1}_{2u',2v'}, \quad (6)$$

$$DOE_{u',v'} = D^{\#1}_{2u',2v'+1}, \quad (7)$$

$$DEO_{u',v'} = D^{\#1}_{2u'+1,2v'}, \quad (8)$$

$$DEE_{u',v'} = D^{\#1}_{2u'+1,2v'+1}, \quad (9)$$

where

$$\begin{cases} u' = 0, 1, 2, ..., (M/2)-1 \\ v' = 0, 1, 2, ..., (N/2)-1 \end{cases}.$$

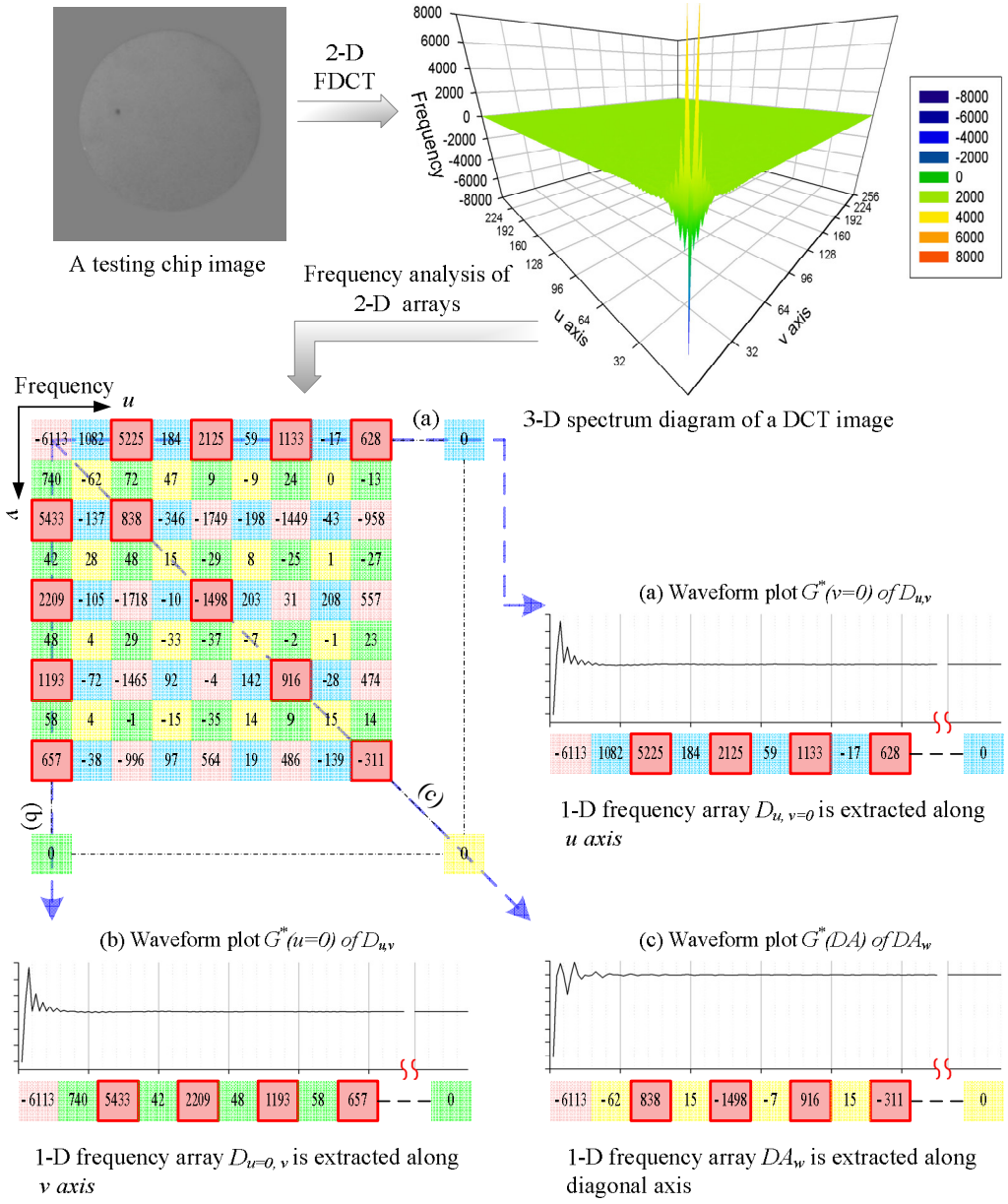

Figure 4. The example of the first stage of the proposed decomposition procedure in DCT domain.

Besides, to obtain the right sector radiuses that will help improve the analysis results, the -45℃ diagonal coefficients of the frequency matrix can be decomposed into a 1-D array DA_t when M and N are equal and the top left DC location is the origin. This diagonal matrix can be denoted as follows:

$$DA_t = D_{t,t}^{\#1}, \tag{10}$$

where $t = 0, 1, 2, \ldots, M\text{-}1$.

The frequencies of the waveform plot $G^{*}(DA_t)$ of the matrix DA_t fluctuate in the same way as those of the waveform matrices $G^{*}(DO_{0\sim(M-1),v})$ and $G^{*}(DE_{0\sim(M-1),v})$. So, we can further decompose the matrix DA_t into $DAO_{t'}$ and $DAE_{t'}$ matrices. These two matrices can be denoted as follows:

$$DAO_{t'} = DA_{2t'}, \tag{11}$$

$$DAE_{t'} = DA_{2t'+1}, \tag{12}$$

where

$$t' = 0, 1, 2, \cdots, (M/2)-1.$$

Based on the aforementioned theoretic deduction and the calculations on the testing images, we propose a two-stage decomposition procedure. In the first stage, a 2-D DCT frequency matrix is broken into multiple 1-D matrices as shown in Figure 4.

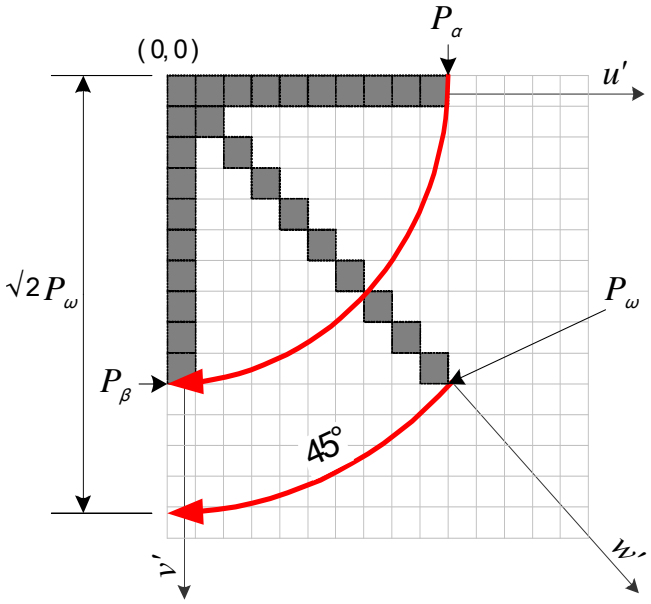

Figure 5. A sector radius diagram obtained from transformation of the three principal frequency arrays.

The purpose of the first stage is to simplify the matrices and use waveform plot G^* to examine how the frequencies of the simplified matrices fluctuate to identify the main properties of the 2-D DCT domain. Then, according to the properties identified, three frequency matrices that represent best, how the frequencies fluctuate are extracted from the 1-D arrays. Take for example a 2-D DCT matrix with size M by M. After the first stage of decomposition, there will be only (M × 3) sets of 1-D frequency arrays left. The second stage of the two-stage decomposition procedure intends to further decompose the three sets of the 1-D frequency arrays produced from the first stage to obtain principal matrices for frequency trend analysis. In the second stage, each 1-D frequency array is divided into two 1-D arrays: one odd and one even.

After completing the two-stage decomposition procedure, frequency fluctuation trends of the waveform plots G^* of the four decomposed frequency matrices were examined as shown in Equations 6 to 9. The waveform plots of the 1-D odd arrays show significant and systematic spectrum changes. The frequency fluctuation trends of the odd-odd matrix are smoother and more predictable when compared with those of the other decomposed matrices. The DCT frequency matrix $D^{\#1}_{u,v}$ needs to be decomposed because most of the regular waveform plots come from the decomposed odd-odd matrix $DOO_{u',v'}$. Therefore, the odd-odd frequency matrix $DOO_{u',v'}$ (including the diagonal matrix $DAO_{t'}$) will be the main target of the later analyses.

Cumulative sum (CUSUM) control scheme

Suppose that Z sample sets with sample size n = 1 are collected and X_z is the observation of the z-th sample, where z = 1, 2, 3, …, s, …, Z. The CUSUM scheme works by accumulating derivations from μ_0 that are above target with one statistic C_s^+ and accumulating derivations from μ_0 that are below target with another statistic C_s^-. The statistics C_s^+ and C_s^- are respectively called one-sided upper and lower CUCUMs. They are computed as follows (Montgomery, 2009):

$$C_s^+ = \max\left[0,\ X_s - (\mu_0 + K) + C_{s-1}^+\right], \quad (13)$$

$$C_s^- = \max\left[0,\ (\mu_0 - K) - X_s + C_{s-1}^-\right], \quad (14)$$

where

$$C_0^+ = C_0^- = 0, \quad K = \frac{\delta}{2}\sigma.$$

In Equations 13 and 14, K is usually called the reference value, and it is often chosen about halfway between the target μ_0 and the out-of-control value of the mean μ_1 that we are interested in detecting quickly. Thus, if the shift is expressed in standard deviation units as $\mu_1 = \mu_0 + \delta\sigma$, then K is one-half the magnitude of the shift. Note that C_s^+ and C_s^- accumulate deviations from the target value μ_0 that are greater than K, with both quantities reset to zero on becoming negative. If either C_s^+ or C_s^- exceeds the decision interval H, the process is considered to be out-of-control. A reasonable value for H is four or five times the process standard deviation σ (Montgomery, 2009).

Reverse order CUSUM method (R-CUSUM)

To detect the transition points in the gentle curves, this research proposes the CUSUM algorithm, which is commonly used in statistical process control to detect the slight shift or deviation from the normal production process. Generally, the CUSUM method processes data, that are smooth in the beginning periods and that deviate slightly in the later periods. However, since the curves fluctuate sharply in the beginning periods and then turn smooth in the other periods, our algorithm applies the reverse order CUSUM method, which processes data in the reverse direction.

The data sequence should be arranged in a reverse order before the reverse-order CUSUM method is applied. According to the definition of CUSUM as shown in Equations 13 and 14, we assume C_z^+ and C_z^- as the one-sided upper and lower CUSUMs of the sequence X_z, respectively. We must substitute the data of the three decomposed frequency matrices $DOO_{u',0}$, $DOO_{0,v'}$ and $DAO_{t'}$ into the sequence X_z^*, respectively, before applying the proposed reverse-order CUSUM method. Then, from the situations of being within or beyond a decision interval H, we determine the status of the process variation and identify the transition points $P(DOO_{u',0})$, $P(DOO_{0,v'})$ and $P(DAO_{t'})$ of the three frequency matrices.

The first value in each of the three frequency matrices $DOO_{u',0}$, $DOO_{0,v'}$ and $DAO_{t'}$ is the DC value in a DCT domain. This value represents the average gray level of an image and is usually the extreme value (the largest or the smallest) in a frequency matrix. Hence, this research sets the DC value at zero when detecting the transition points in the gentle curves to determine the proper radius of the sector filter.

Setting the DC value at zero will avoid significant variations among the frequency components. After the calculations in Equations 13 and 14, three transition points will be identified in the gentle curves by the R-CUSUM method. The proper radius of the sector filter R^* can be denoted as:

$$R^* = 2AVG(P_\alpha, P_\beta, P_\omega) + 1, \quad (15)$$

where

$$AVG\ (P_\alpha, P_\beta, P_\omega) = average\ (P_\alpha, P_\beta, \sqrt{2}P_\omega).$$

The calculation of the proper radius R^* is presented in Equation 15, where three transition points are used. Figure 5 shows points P_α,

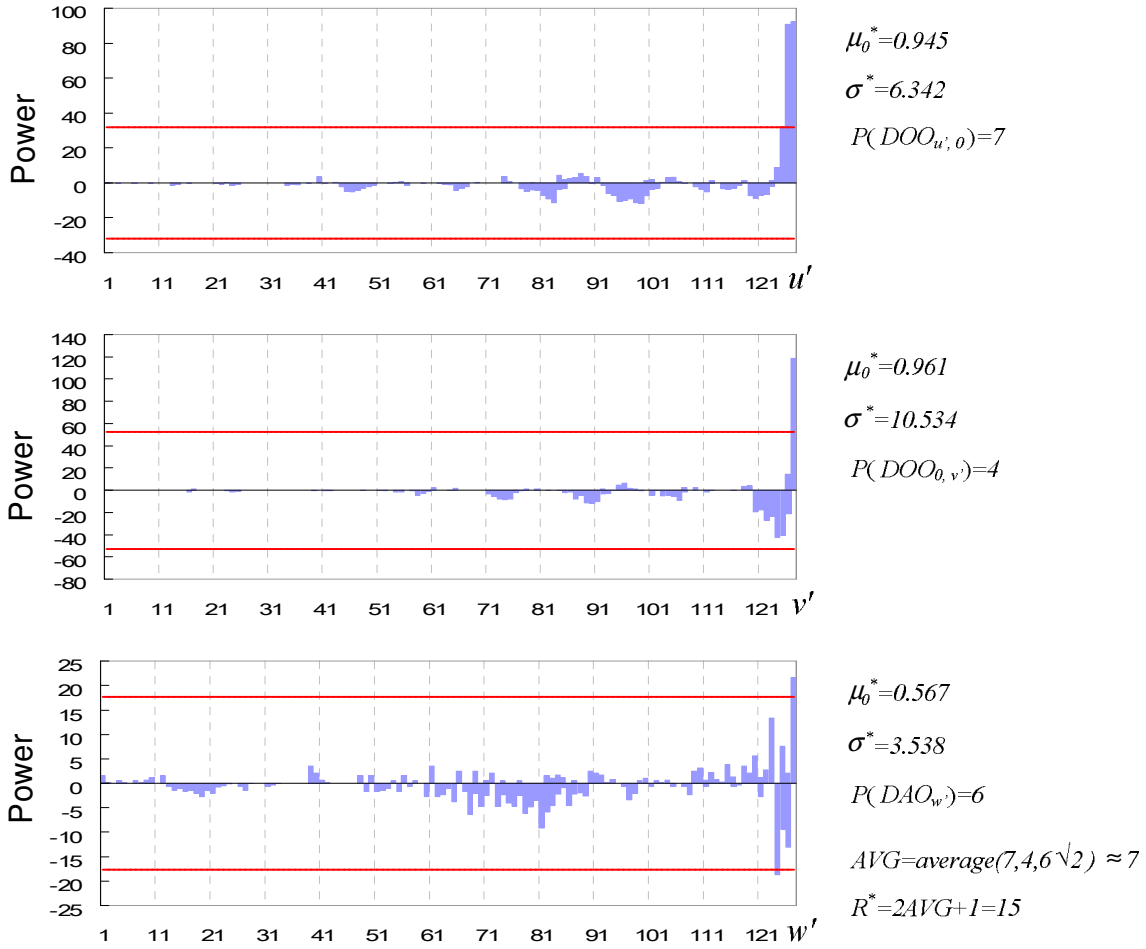

Figure 6. Calculation of the filter radius R* by the R-CUSUM method.

P_β and P_ω are the three transition points of the gentle curves along *u'*, *v'* and diagonal axes, respectively. The point P_ω must be multiplied by a weight of $\sqrt{2}$, because this point comes from the diagonal matrix $DAO_{t'}$ and must be adjusted to be in the same scale as P_α and P_β. And then, the three transition points are substituted into Equation 15 to compute the best filter radius *R**. Figure 6 shows the calculation of the best filter radius *R** by the R-CUSUM method.

Image restoration and defect segmentation

Figure 7 shows the whole process of the proposed DCT based enhancement approach for micro flaw detection on electronic chips. A testing image with micro flaws which are difficult to detect in the spatial domain is processed by the proposed DCT high-pass filtering operation. Then, taking the inverse DCT of the filtered result, we can have the micro defects easily segmented by the Kapur's entropy method (Kapur et al., 1985).

The Kapur's entropy method regards the image foreground and background as two different signal sources, so when the sum of the entropies of the two signal sources reaches its maximum, the image is said to be an optimal threshold (Kapur et al., 1985). Let us consider an image with gray levels in the range [0, *L*-1]. We assume S_l be the number of pixels in the image having gray level *l* and the total number of pixels in the image should be $\sum_{l=0}^{L-1} S_l$. Then, Y_l is an estimate of the probability of occurrence of gray level *l* in the image, denoted as $Y_l = S_l / \sum_{l=0}^{L-1} S_l$. From the definition of entropy, the entropy of an image is $N = -\sum_{l=0}^{L-1} Y_l \ln Y_l$. We aim to classify the pixels of the image into two opposite classes, namely flaw (black) and normal region (white) by thresholding. The entropy of the defective portion of an image is $N_O(T)$ and the entropy of the normal portion of an image is $N_B(T)$. Therefore, the Kapur's entropy method is to determine the value of the threshold *T*, such that the total entropy *N*, as defined in Equation 16, of the partitioned image is maximized.

$$N = N_O(T) + N_B(T) = -\sum_{r=0}^{T} Y_r \ln Y_r - \sum_{r=T+1}^{L-1} Y_r \ln Y_r \quad (16)$$

The Kapur's entropy method outperforms many other methods in detecting small objects (Sezgin and Sankur, 2004). However, the

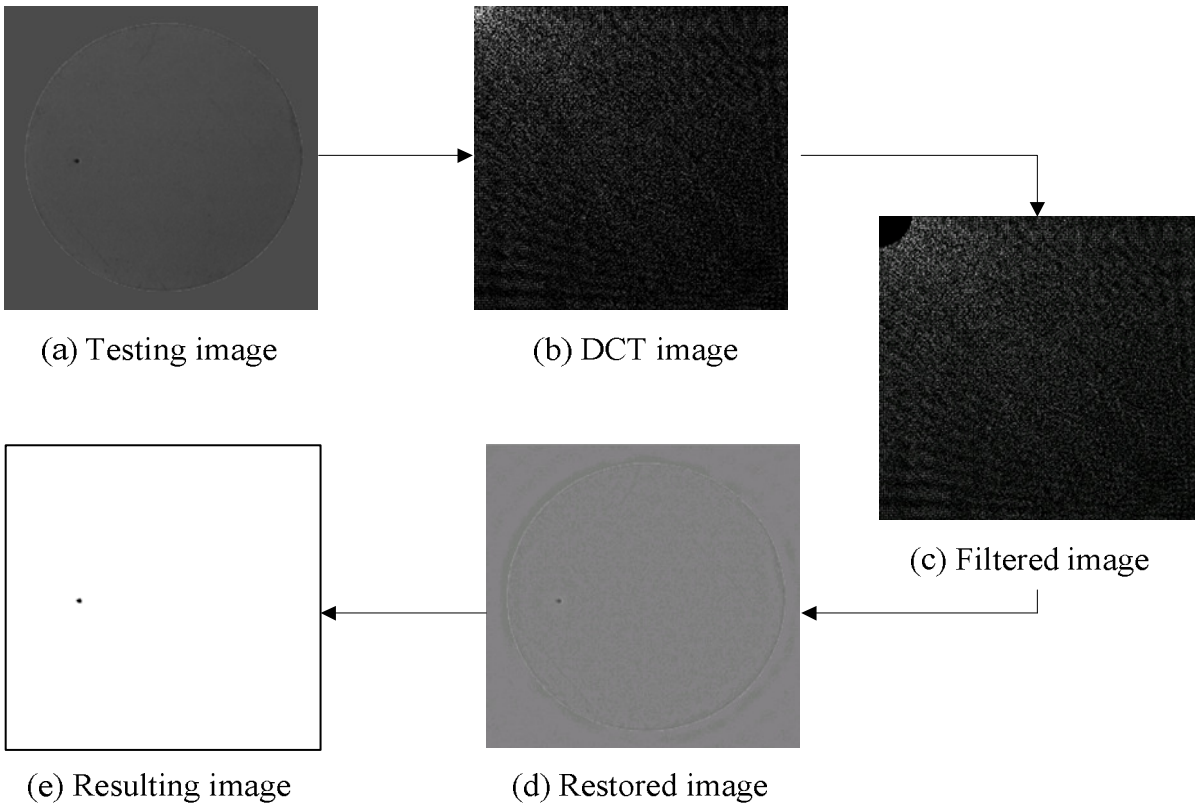

Figure 7. Micro flaw detection procedure diagram of the DCT based enhancement approach.

entropy method cannot correctly separate micro flaws if the chip image does not go through the defect enhancement step of the proposed DCT frequency filtering operation. This is because many noises in the image may incur erroneous judgement in flaw separation. If an image is processed by the proposed DCT-based image reconstruction approach in advance, the surface micro flaws in the image can be precisely located by the Kapur's entropy method.

RESULTS AND DISCUSSION

Implementation and analyses

Here, we implement the proposed approach and conduct experiments to evaluate its performance in detecting surface micro flaws of the electronic chips. To strengthen the visibility of the surface flaws, we make use of the following equipments: a white ring LED lighting device, a charge-coupled device (CCD) camera model WAT-221S of Watec Company, a lens with 1 to 10 amplifications of changeable focal lengths, a frame grabber model IMAQ PCI-1411 of National Instruments Corporation and a XYZ electronic control table with a controller. Figure 8a demonstrates the configurations of the experimental environment in which we scan real electronic chips to be used as testing samples and Figure 8b shows the user interface of the developed software. Each image of the chip has a size of 256 × 256 pixels and a gray level of 8 bits. In the experiments with large samples, 100 images are defective chips with one or more than one micro flaws and the other 20 images are regular chips without any micro flaw. The micro flaw detection algorithm is edited in C language and executed on the sixth version of the C++ Builder complier on a personal computer (Pentium-4 2.8 GHz and 1 GB DDRII 667 Hz-RAM).

The performance evaluation indices, (1-α) and (1-β), are used to represent correct detection judgments; the higher the two indices, the more accurate the detection results. Statistical type I error α suggests the probability of producing false alarms, that is, detecting normal regions as flaws. Statistical type II error β implies that the probability of producing missing alarms, which fail to alarm real flaws. We divide the area of normal region detected as flaws by the area of actual normal region to obtain type I error, and the area of undetected flaws by the area of actual flaws to obtain type II error. Therefore, the correct classification rate (CR) is defined as:

$$CR = (N_{cc} + N_{dd}) / N_{total} \times 100\% , \quad (17)$$

Where N_{cc} is the pixel number of normal textures detected as normal areas, N_{dd} is the pixel number of

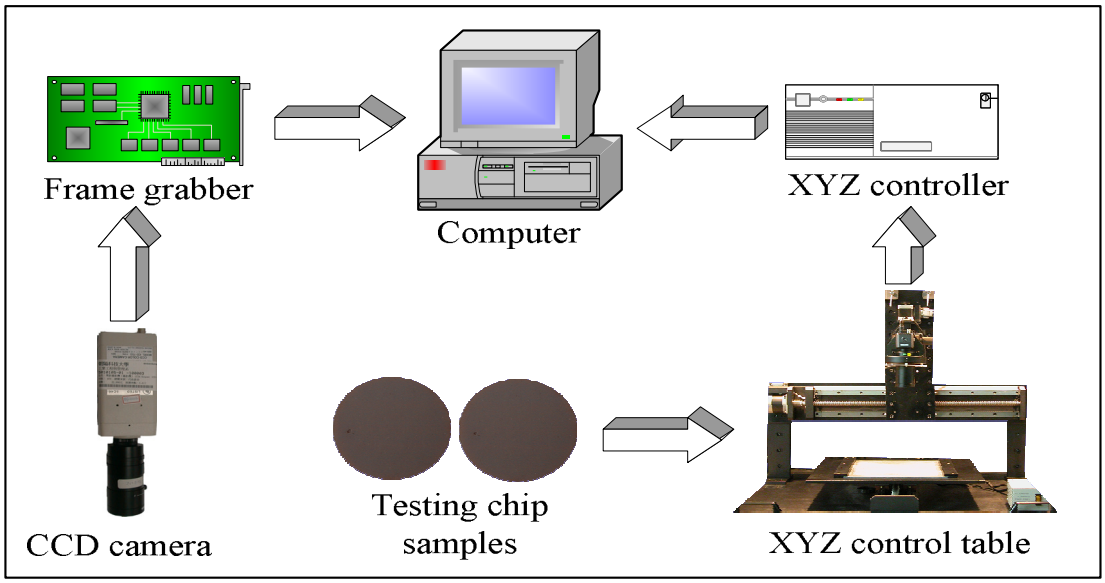

(a)

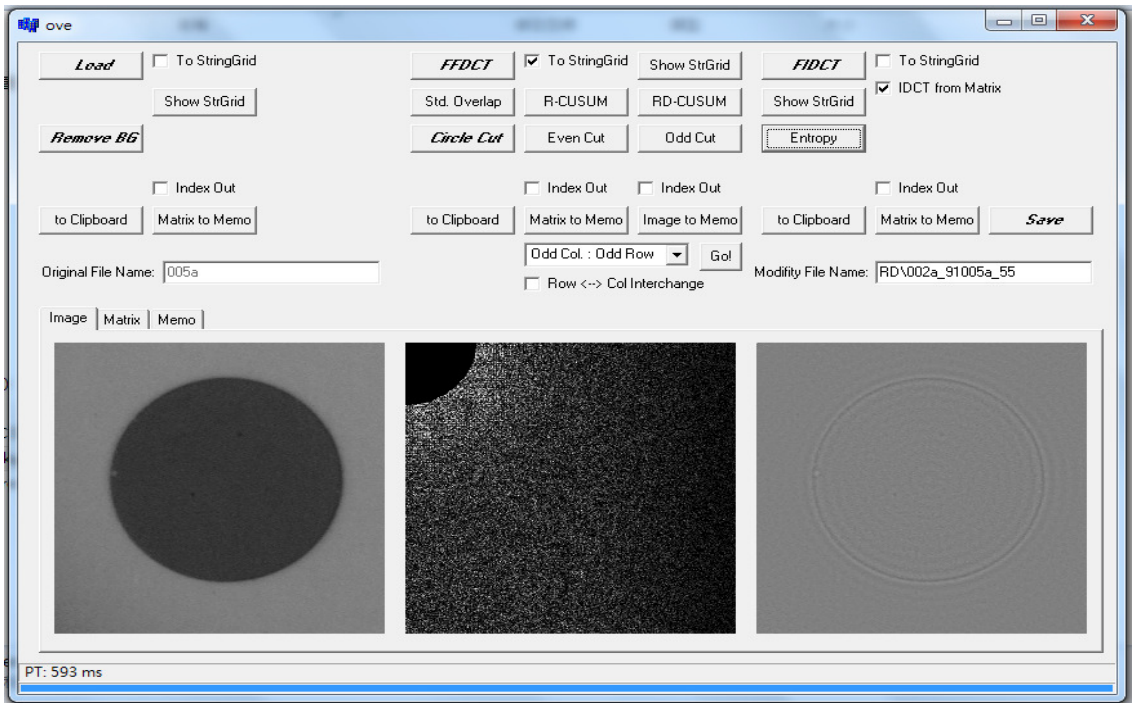

(b)

Figure 8. Experimental configuration and user interface of the developed system: (a) Hardware setup of the conducted experiments; (b) User interface of the developed software.

flaws detected as defective regions and N_{total} is the total pixel number of a testing image.

To demonstrate the flaw detection results, Figure 9 lists partial results of detecting surface micro flaws by the Otsu method (Otsu, 1979), the iterative method (Jain et al., 1995), the Kapur's entropy method (Kapur et al., 1985), the proposed method and the professional inspector, individually. The three spatial domains techniques, the iterative, Otsu and Kapur's entropy methods, make lots of erroneous judgments (false alarms) on micro flaw detection. The frequency domain technique, the proposed method, detects most of the micro flaws and makes less erroneous judgments.

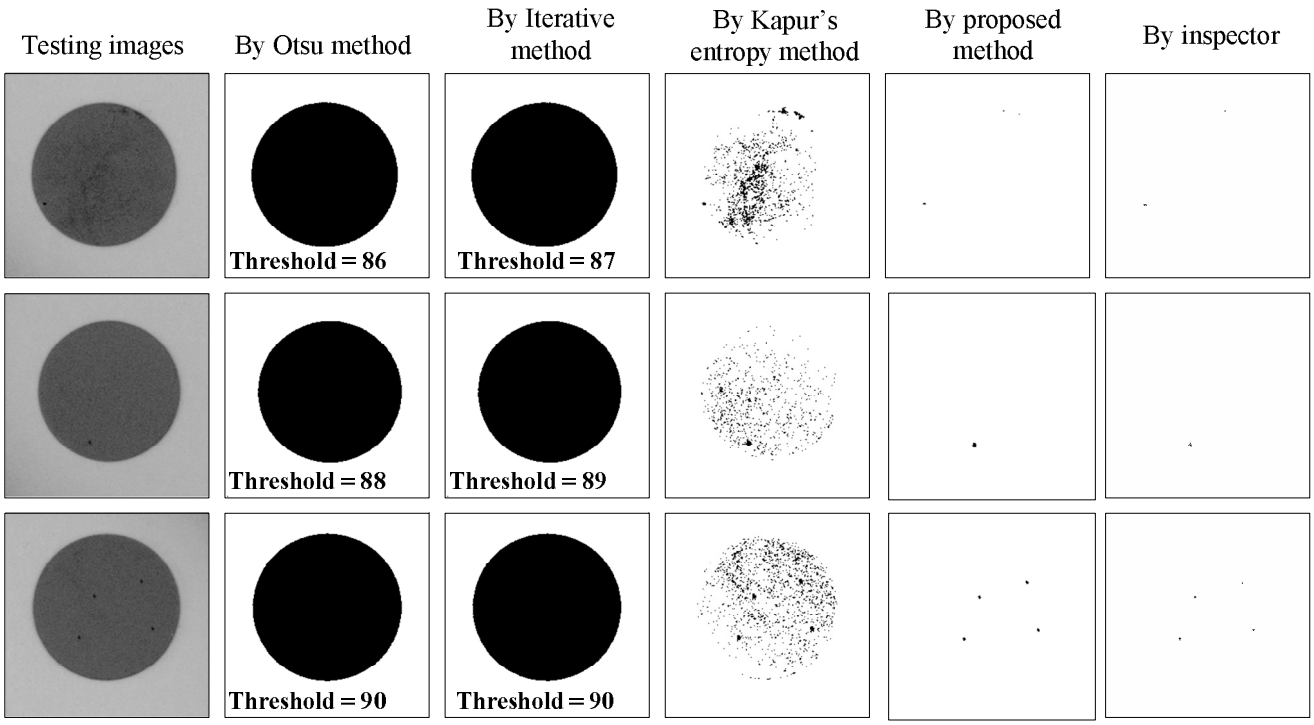

Figure 9. Partial detection results of the Otsu, iterative, Kapur's entropy, the proposed methods and inspector.

Table 1. Summarized comparison table of surface micro flaw detection of electronic chips for four different methods.

Parameter	Otsu method	Iterative method	Kapur's entropy method	Proposed method
1-β (%)	99.99	99.99	98.88	96.24
α (%)	46.64	46.26	8.08	0.15
CR (%)	54.26	54.73	92.64	99.67
Time (s)	0.55	0.62	0.72	2.48

Therefore, the frequency domain approach outperforms the spatial domain techniques in the surface micro flaw detection of the electronic chips.

To compare the performance of the surface micro flaw detection, Table 1 summarizes the detection results of our experiments. Three spatial domain approaches and one frequency domain techniques are evaluated against the results by professional inspectors. The average defect detection rates (1-β) of all testing samples by the four methods are, respectively, 99.99% (Otsu method), 99.99% (iterative method), 98.88% (Kapur's entropy method) and 96.24% (the proposed method). To rigorously justify the detection performance of the proposed method, a statistical hypothesis testing is applied to test the significance of the 96.24% probability of correctly discriminating micro flaws from normal regions. The result of Z-test with large-sample tests on a proportion (Montgomery and Runger, 2007) concludes that it is significant (with p-value 0.022) that the micro flaw detection rate is not less than 96.24% at 95% confidence level. However, the three spatial domain methods have significantly higher false alarm rates (α), 46.64% (Otsu method), 46.26% (iterative method) and 8.08% (Kapur's entropy method). On the contrary, the other frequency domain approach has rather lower false alarm rate, 0.15% (proposed method). The proposed method has higher correct classification rates (CR) than do the other methods applied to micro flaw detection of electronic chip images. The average computation time for processing an image of 256 × 256 pixels is as follows: 0.55 s by the Otsu method, 0.62 s by the iterative method, 0.72 s by the Kapur's entropy method and 2.48 s by the proposed method. Hence, the proposed method can overcomes the difficulties of detecting small defects on electronic chips and excels in its ability of correctly discriminating micro flaws from normal regions.

Conclusion

This research proposes a new approach that applies DCT based enhancement for the detection of micro flaws on electronic chips. This approach does not require pre-stored texture images for reference or any texture information of a faultless sample chip. Real electronic chips are used as testing samples and experiments with large samples are conducted in a practical inspection environment to verify the performance of the proposed approach. Experimental results demonstrate that the proposed approach is invariant to the orientation of the target chip and achieves high accuracy in detecting surface micro flaws. Besides, the proposed chip surface inspection algorithm is easy to implement and does not require a primitive-matching process. Therefore, the proposed approach can be further applied to detect surface microflaws of various types of electronic and optical components that are similar to the electronic chips.

In the processing time of the proposed approach, the time of taking forward and inverse DCT needs about 2 s on average without doing any parameter optimization in the transformation. This processing time will be significantly shortened after the parameter optimization is conducted and the DCT implemented in a single integrated circuit. If we do not count the time of taking forward and inverse DCT, the time of taking the R-CUSUM method is less than 50 m/s and the processing time of each method is very time-saving. The proposed method effectively and efficiently overcomes the difficulties of detecting small defects on electronic chip images with random textured surfaces and excels in its ability of correctly discriminating micro flaws from normal regions.

ACKNOWLEDGEMENT

This work was partially supported by the National Science Council (NSC) of Taiwan, under Grant No. NSC 94-2221-E-324-001.

REFERENCES

Ahmed N, NatarajanT, Rao KR (1974). Discrete cosine transform. IEEE Trans. Comput., 23: 90-93.

Chan CH, Pang GKH (2000).Fabric defect detection by Fourier analysis. IEEE Trans. Ind. Appl., 36: 1267-1276.

Chen B, LatifiS, Kanai J (1999). Edge enhancement of remote sensing image data in the DCT domain. Image Vision Comput., 17(12): 913-921.

Chen WH, Smith CH, Fralick SC (1977). A fast computational algorithm for the discrete cosine transform. IEEE Trans. Commun., 25(9): 1004-1009.

Cho NI, Lee SU (1991). Fast algorithm and implementation of 2-D discrete cosine transform. IEEE Trans. Circuits Syst., 38(3): 297-305.

Gonzalez RC, Woods RE (2008).Digital Image Processing, 3rd Ed., Prentice Hall, New Jersey, USA.

Jain R, Kasturi R, Schunck BG (1995).Machine Vision. International Editions, McGraw Hill, New York, NY, USA.

Kapur J, Sahoo P, Wang A (1985). A new method for gray-level picture thresholding using the entropy of the histogram. Computer Graphics Image Process, 29: 273-285.

Kim YT (1997).Contrast enhancement using brightness preserving bi-histogram equalization.IEEE Trans. Consum. Electron., 43: 1-8.

Kim SY, Han D, Choi SJ, Park JS (1999).Image contrast enhancement based on the piecewise-linear approximation of CDF. IEEE Trans. Consum. Electron., 45(3): 828-834.

Kumar A (2008).Computer-vision-based fabric defect detection: a survey. IEEE Trans. Ind. Electron., 55(1): 348-363.

Lin HD (2007). Automated visual inspection of ripple defects using wavelet characteristics based multivariate statistical approach. Image Vision Comput., 25: 1785-1801.

Lin HD, Chiu YP, Hsu SY (2011). A visual inspection system for quality control of optical lenses.Int. J. Phys. Sci., 6(11): 2701-2709.

Mak KL, Peng P, Yiu KFC (2009). Fabric defect detection using morphological filters. Image Vision Comput., 27(10): 1585-1592.

Montgomery DC (2009). Statistical Quality Control: A Modern Introduction.6th Edition, John Wiley & Sons, New York, NY, USA.

Montgomery DC, Runger GC (2007).Applied Statistics and Probability for Engineers.4th Edition, John Wiley & Sons, New York, NY, USA.

Ngan HYT, Pang GKH, Yung NHC (2011). Automated fabric defect detection-a review. Image Vision Comput., 29: 442-458.

Ngo CW, Pong TC, Chin RT (2001). Exploiting image indexing techniques in DCT domain. Pattern Recognit., 34: 1841-1851.

Otsu N (1979).A threshold selection method from gray level histogram.IEEE Trans. Syst. Man Cybern. Part B Cybern., 9: 62-66.

Ruzon MA, Tomasi C (2001).Edge, junction, and corner detection using color distributions.IEEE Trans. Pattern Anal. Mach. Intell., 23(11): 1281-1295.

Sezgin M, Sankur B (2004). Survey over image thresholding techniques and quantitative performance evaluation.J. Electron. Imaging, 13(1): 146-165.

Tsai DM, Hsiao B (2001).Automatic surface inspection using wavelet reconstruction. Pattern Recognit., 34: 1285-1305.

Wu WY, Wang MJ, Liu CM (1996).Automated inspection of printed circuit boards through machine vision. Comput. Ind., 28: 103-111.

Zhong Y, Jain AK (2000).Object localization using color, texture and shape. Pattern Recognit., 33: 671-684.